Isobaric vapour-liquid equilibrium of α-terpineol highly diluted in hydroalcoholic mixtures at 101.3 kPa: Experimental measurements and thermodynamic modeling

Gabriela Zanghelini, Violaine Athès, Martine Esteban-Decloux, Pierre Giampaoli, Stéphane Vitu

Isobaric vapor-liquid equilibrium of α-terpineol highly diluted in hydroalcoholic mixtures at 101.3 kPa: experimental measurements and thermodynamic modeling

Gabriela Zanghelini[a,*], *Violaine Athès*[a], *Martine Esteban-Decloux*[a], *Pierre Giampaoli*[a] *and Stéphane Vitu*[a,b]

[a]Université Paris-Saclay, INRAE, AgroParisTech, UMR SayFood, 91300 Massy, France

[b]CNAM, 75003 Paris, France

ABSTRACT

Terpenes are important varietal compounds responsible for the characteristic aromas of alcoholic beverages. Reliable vapor-liquid equilibrium (VLE) data for this class of aroma compounds in hydroalcoholic media is essential to understand their behavior during distillation and thus achieve a desired quality in the distilled products. In this work, experimental measurements for the VLE of α-terpineol highly diluted in ethanol-water mixtures were carried out in a recirculation ebulliometer operating at 101.3 kPa for boiling temperatures from (354.99 to 369.93) K. Equilibrium compositions were determined by gas chromatography for α-terpineol and by density measurements for ethanol. Results show that α-terpineol is expressively more volatile in the dilute region ($x_{Et} < 0.01$), where it can be up to 30 times more abundant in the vapor phase and twice as volatile as ethanol. Inversely, when $x_{Et} > 0.15$ α-terpineol can be 10 times richer in the liquid phase. The experimental data were correlated by semi-empirical models NRTL and UNIQUAC and compared with predictions by UNIFAC. The data regressed with the NRTL model showed the best agreement with the experimental data. The binary interaction parameters fitted by the model are suitable to be used in the design and simulation of distillation processes for the production of alcoholic beverages.

Keywords: vapor-liquid equilibrium, infinite dilution activity coefficient, alpha-terpineol, hydroalcoholic mixture, NRTL, UNIQUAC.

1. INTRODUCTION

Alcoholic beverages are essentially highly non-ideal hydroalcoholic mixtures containing hundreds of highly diluted aroma compounds, also known as congeners. Ethanol and water are the major compounds, accounting for approximately 96% of the total mass[1], whereas congeners are present at trace amounts (with mass fractions between 10^{-10} and 10^{-3}) and cover several chemical families including alcohols, carboxylic acids, aldehydes, norisoprenoids, esters and terpenes. Despite their low concentration, congeners are passible of volatilizing into the headspace where they can impart odor notes that vary in quality and intensity and build up the characteristic aroma of alcoholic beverages. The olfactory impact of an aroma compound depends on its distribution between the vapor and liquid phases, or absolute volatility, as well as physical, chemical and structural properties of each component in a mixture and the interactions between them[2,3]. Understanding the intricate interactions between the different species in a system and their behavior during processing is essential to achieve a desired quality in the product.

Amongst odorant compounds in wines and distilled beverages, terpenes are a large class of volatile compounds of various structural types, including monoterpenes (C_{10}) and sesquiterpenes (C_{15}). Often associated with floral notes, terpenes are important varietal compounds responsible for the characteristic aromas of wine, where they are present as volatile aglycones or non-volatile glycosides[4,5]. One of such aglycones is α-terpineol, a natural monoterpene present in grapes and wine that is considered a discriminant compound between white wines typically used for distillation[6]. It has been detected in cachaça[7], pisco[8] and in French spirits cognac[9], calvados and armagnac[10], and is deemed to play a major role in the aroma of gin[11], tequila[12] and grappa[13].

In spirit distillation, congeners are extracted from the wine or fermented base and concentrated along with ethanol in the distillate fractions. Not all aroma compounds are desirable in the distillate, as some of them are associated with deleterious odors or a level of toxicity that might hamper the quality of the final product. Thereby, the challenge of distillation lies in achieving a balance between the concentrations of pleasant and undesirable odorant compounds in the distillate, which in turn requires a thorough knowledge of the behavior of the system and its components. Compound separation in

distillation processes is driven by heat-induced deviations of a given state from a state of vapor-liquid equilibrium (VLE). As such, the design and simulation of distillation processes for the production of alcoholic beverages entails accurate knowledge of VLE data for aroma compounds highly diluted in ethanol-water mixtures at the entire composition range. Thermodynamic equilibrium implies an equality of temperature and pressure in the different phases and an equality of fugacities for each species in each phase. Thus, the equilibrium problem unfolds into the measurement and calculation of four variables: temperature, pressure and compositions of the vapor and liquid phases.

Because distillation is most often carried out at atmospheric pressure (~101.3 kPa), equilibrium is generally modeled following the gamma-phi approach, in which the vapor phase is described by equations of state and the non-ideality associated with the liquid phase is expressed by activity coefficient models, also known as molar excess Gibbs energy models[14–17]. Given the low concentrations of congeners in the wine and distillate, their influence in the thermodynamic behavior of the ethanol-water mixture is negligible and their interactions with the hydroalcoholic matrix are characterized by infinite-dilution activity coefficients (γ_i^{∞}), also referred to as limiting activity coefficients[1]. Reliable experimental values of γ_i^{∞} allow to accurately describe VLE in the dilute regions of a mixture and can be correlated by thermodynamic models to predict VLE over the entire composition range[18,19] and estimate binary interaction parameters that can be applied for process simulation.

Thermodynamic models that are suitable for low-pressure VLE of ethanol + water + congener mixtures include predictive models such as UNIFAC[20] and PSRK[21] and semi-empirical models such as Wilson[22], NRTL[23,24] and UNIQUAC[25]. While the first are entirely predictive models, the latter are correlating models, meaning that they require experimental VLE data to calculate certain empirical parameters and binary interaction parameters. However, the availability of such data in the literature is rather scarce for some systems, as is the case for multicomponent mixtures in the dilute region, especially for aroma compounds in aqueous media. Although predictive methods can be useful tools to represent VLE when empirical data is not available, they have been shown to provide limited accuracy for binary and multicomponent mixtures[26]. As a result, experimental

measurements of infinite dilution activity coefficients still prove needed to accurately characterize the behavior of volatile compounds throughout distillation.

Despite the prominent role of terpenes in the typicality of wine distillates, the number of studies involving VLE data for terpenes in hydroalcoholic media is rather scarce in the literature. Low-pressure VLE data have been reported for some terpenes highly diluted in ethanol-water mixtures, including linalool (CAS no. 78-70-6)[27,28] and α-pinene (CAS no. 80-56-8), D-limonene (CAS no. 5989-27-5) and (*Z*)-linalool oxide (CAS no. 60047-17-8)[28]. Additionally, infinite-dilution activity coefficients and vapor pressures have been provided in the literature for various terpene + water binary systems at 298.15 K, including α-terpineol + water[29]. To our knowledge, no VLE data has been reported in the literature for the system α-terpineol + ethanol + water.

This work focuses on the experimental acquisition of VLE data at 101.3 kPa for α-terpineol highly diluted in ethanol-water mixtures for a temperature range from (354.99 to 369.93) K. The experimental apparatus is a Gillespie-type recirculation ebulliometer operating at adiabatic and isobaric conditions[30] and compositions are determined using a density meter and a gas chromatograph coupled to a flame-ionization detector (GC-FID). The experimental ternary data measured are then used to calculate infinite-dilution activity coefficients and binary interaction parameters for correlating models NRTL and UNIQUAC. The predictive capability of the UNIFAC model for the system is also evaluated.

2. EXPERIMENTAL MEASUREMENTS

2.1. Materials

The chemical compounds used in this work with their respective mass fraction purities, CAS numbers and some of their pure component properties are listed in Table 1. Deionized water (resistivity 18.2 MΩ-cm at 25 °C) was obtained from a Milli-Q purification system (Simplicity 185, Millipore Waters, France). For the VLE measurements, the different hydroalcoholic mixtures were prepared by precisely weighing ethanol, water and α-terpineol with a resolution of ±0.001 g (EG420-3NH, Kern). Ethanol mole fractions ranged from x_{Et} =

($1.6 \cdot 10^{-2}$ to $3.0 \cdot 10^{-1}$) (or from w_{Et} = ($4.0 \cdot 10^{-2}$ to $5.2 \cdot 10^{-1}$) in mass fractions) and the mole concentration of α-terpineol in the initial solutions was fixed at $1.0 \cdot 10^{-4}$, which corresponds to a mass composition ranging from $w_{\alpha T}$ = ($6.5 \cdot 10^{-4}$ to $8.4 \cdot 10^{-4}$).

Table Erreur ! Il n'y a pas de texte répondant à ce style dans ce document.**.** Specifications and physical properties of the aroma compounds used in this work: molecular mass (MM/g·mol^{-1}), normal boiling point (T_b/K) at 101.3 kPa, $\log_{10}$ of the octanol/water partition coefficient at T = 298.15 K (log K_{ow}).

Compound	α-terpineol	ethanol	water
CAS	98-55-5	64-17-5	7732-18-5
Formula	$C_{10}H_{18}O$	C_2H_6O	H_2O
Structure	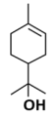		
Supplier	BOC Sciences	Carlo Erba	
Mass fraction purity	≥0.969[a]	≥0.999[a]	
MM/g·mol^{-1}	154.25	46.07	18.01
T_b/K exp.		351.45[b]	373.15[b]
lit.	492.95[c]	351.44[d,e,f], 351.48[g], 351.45[h]	373.15[d,e,f,g,h]
log K_{ow}	2.98[i]	-0.31[j]	-1.38[j]

[a]determined by gas chromatography by the supplier. [b]This work, measured at 101.3 kPa ($u(T_b)$ = 0.2 K, $u(P)$ = 0.5 kPa). [c]DIPPR database, available in the ProSim software[31]. [d]Arce et al., 2007[32]. [e]Kamihama et al., 2012[33]. [f]Riddick et al., 1986[34]. [g]Kojima et al., 1968[35]. [h]Lai et al., 2014[36]. [i]Li & Perdue, 1998[37]. [j]Hansch et al., 1995[38].

2.2. Experimental VLE measurements

Vapor-liquid equilibrium measurements were carried out in a Gillespie-type recirculation still (Labodest VLE 602, iFisher GmbH, Germany) operating at isobaric and adiabatic conditions. The equipment has been used by our research team in the past years for VLE measurements of other aroma compounds[27,28,39] and its principle has been thoroughly described in the literature[27,40–42]. System pressure is assessed by a digital manometer with an accuracy of ±0.5 kPa (P-10 WIKA, iFisher GmbH, Germany) and the temperatures of liquid and vapor phases in the separation chamber are measured by a Pt-100 platinum

probe with an accuracy of ±0.05 K, periodically calibrated against a reference probe (Pt-100 RTD 712, Fluke, France). A schematic diagram of the apparatus is provided in Figure 1.

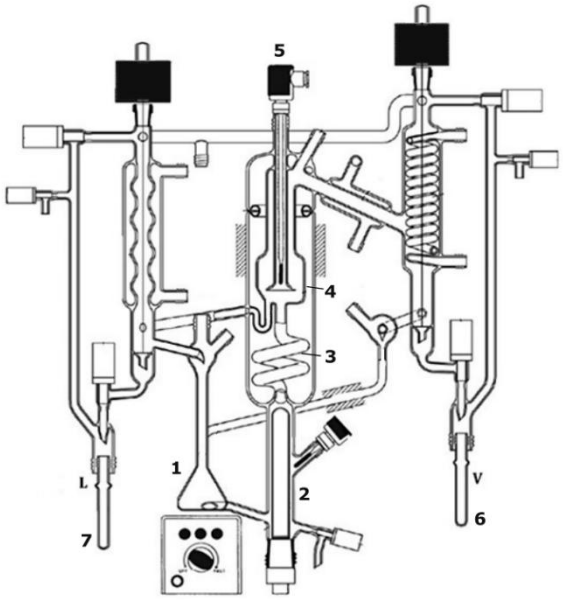

Figure 1. Schematic diagram of the Labodest VLE 602 (iFischer) system: (1) mixing chamber, (2) boiler, (3) "Cottrell pump" or equilibrium chamber, (4) separation chamber, (5) Pt-100 temperature probe, sampling tubes for the (6) vapor and (7) liquid phases.

Eighteen independent equilibrium assays were conducted, during which pressure was maintained at 101.3 kPa under inert nitrogen atmosphere. For each run, 85 mL of mixture are inserted in the mixing chamber (1) and brought to a boil by a glass quartz immersion heater (2). Rising vapors transporting some liquid droplets flow through the Cottrell pump (3), in which the vapor and liquid phases remain in intimate contact and maximum mass transfer is assured, then enter the separation chamber (4). The liquid and condensed vapor are separately recycled into the mixing chamber, where the mixture is under constant stirring. Equilibrium is considered to be reached when vapor temperature remains stable (±0.1 K) for 30 minutes. A small amount of sample (2 mL) is then collected through the sampling tubes (6,7) for each phase for analysis.

2.3. Determination of equilibrium compositions

The compositions of the liquid and condensed vapor phases were determined by density measurements, followed by gas chromatography. Density measurements were carried out in an Anton Paar oscillating tube density meter (DMA 4500 M, Anton Paar) set to 25 °C with a resolution of (±0.00001) $g \cdot cm^{-3}$. A two-point calibration of the device was performed regularly using pure degassed water and dry air. The ethanol mass fractions were determined from the density measurements using the mathematical model developed by Wagenbreth and Blanke[43] and reported by the International Organization of Legal Metrology (OIML)[44]. The model is based on experimental density data measured by different national metrology laboratories for different ethanol-water mixtures valid for temperatures from (-20 to 40) °C. The accuracy of the density measurements and determination of ethanol concentrations was verified by measuring the density of several ethanol-water solutions of known composition and confronting experimental results with the literature. The data is reported in Appendix A.

The concentrations of α-terpineol in the vapor and liquid phases were measured in a gas chromatograph (GC Trace 1300 Series, Thermo Fisher Scientific) equipped with a flame ionization detector and an automatic sampler (TriPlus RSH, Thermo Fisher Scientific). An aliquot of 0.5 μL of the diluted sample was directly injected in splitless mode using a 1 μL precision glass syringe. Inlet and detector temperatures were both set to 250 °C. Helium was used as the carrier gas with a constant flow of 1.2 $mL \cdot min^{-1}$. Hydrogen and air flow for the flame jet were 35 and 350 $mL \cdot min^{-1}$, respectively. The stationary phase was a ZB-Wax Plus °(100% Polyethylene Glycol) capillary column (30 m x 0.25 mm, 0.5 μm) connected to a deactivated fused silica pre-column (1 m x 0.25 mm). The initial oven temperature was set to 80 °C and maintained for 2 min, then increased at a linear rate of 20 $°C \cdot min^{-1}$ to 240 °C and held for 5 min. The total running time was 15 min. The chromatographic data were acquired and analyzed using Chromeleon CDS software version 7.2.10 (Thermo Scientific).

All samples were adjusted to an ethanol mass fraction of w_{Et} = 0.6 before analysis to overcome matrix effects and minimize measurement variability between the different samples. The mass compositions of α-terpineol were determined from calibration curves of the pure component in an ethanol-water mixture at the same ethanol mass fraction of w_{Et} = 0.6. Seven calibration points were established with α-terpineol mass fractions ranging from

$w_{\alpha T}$ = ($2.2 \cdot 10^{-4}$ to $4.1 \cdot 10^{-2}$). Terpinen-4-ol (CAS 562-74-3; Sigma-Aldrich) was added as an internal standard at a fixed concentration of $4.2 \cdot 10^{-3}$ g·g^{-1} to minimize system variability between injections. All injections were performed in triplicate and results were multiplied by a dilution factor accounting for the initial adjustment. The detection and quantitation limits estimated for α-terpineol from the calibration curves were LOD = $3.4 \cdot 10^{-5}$ g·g^{-1} and LOQ = $1.0 \cdot 10^{-4}$ g·g^{-1} (or $6.3 \cdot 10^{-6}$ and $1.9 \cdot 10^{-5}$ in mole fraction, respectively).

2.4. Computation of uncertainties

The standard uncertainties related to experimental measurements were calculated according to the law of propagation of uncertainty. Sources of uncertainty considered include mass fraction purity, the mass measurements, the density determination, the temperature and pressure measurements and the repeatability of chromatographic analyses (based on three injections). The calculated values are presented with the experimental data in the results section and in the appendix.

3. THERMODYNAMIC MODELING

This section explores the basic equations of vapor-liquid equilibrium and introduces the thermodynamic models employed in this work. The choice of a suitable thermodynamic model is essential to accurately represent phase equilibria of multicomponent mixtures in the simulation of separation processes.

3.1. Vapor-liquid equilibrium theory

At low pressures (<1000 kPa), VLE can be computed by a modified Raoult's law, in which the vapor phase is considered an ideal gas mixture and all properties of the liquid phase can be presumed pressure independent[15].

The vapor pressure of a pure compound i at a temperature T/K can be calculated from the Riedel equation[45,46]:

$$P_i^0(T)/\mathrm{MPa} = \exp\left(A_i + \frac{B_i}{T} + C_i \ln T + D_i T^{E_i}\right) \#(1)$$

in which A_i, B_i, C_i, D_i, E_i are empirical coefficients specific to each compound. The Riedel coefficients for the studied system are listed in Table 2.

Table 1. Riedel equation coefficients[a] for calculating the vapor pressures of each component in the mixture at a given temperature.

Compound	A_i	B_i	C_i	D_i	E_i	T_{min}/K	T_{max}/K
α-terpineol	79.319	-9967.8	-7.6780	$3.87 \cdot 10^{-18}$	6	309.65	675.00
ethanol	73.304	-7122.3	-7.1424	$2.89 \cdot 10^{-6}$	2	159.05	514.00
water	73.649	-7258.2	-7.3037	$4.17 \cdot 10^{-6}$	2	273.16	647.10

[a]all coefficients were obtained from the DIPPR Database, available in the Simulis Thermodynamics package (ProSim)[31]. T_{min}/K and T_{max}/K define the temperature interval in which the equation coefficients are valid.

The equilibrium behavior of an aroma compound in hydroalcoholic mixtures can be further described by its partition coefficient and its relative volatility. The partition coefficient (K_{AC}), also known as absolute volatility, describes the distribution of an aroma compound (AC) between the liquid and vapor phases at equilibrium, as defined by:

$$K_{AC} = \frac{y_{AC}}{x_{AC}} = \frac{\gamma_{AC}(T, \mathbf{x}) P^0_{AC}(T)}{P} \#(2)$$

The relative volatility of an aroma compound in relation to ethanol ($\alpha_{AC/Et}$) can inform on the behavior of the compound during distillation. It is defined as the ratio of the absolute volatilities of the aroma compound and ethanol, which can be expressed as:

$$\alpha_{AC/Et} = \frac{K_{AC}}{K_{Et}} = \frac{y_{AC}/x_{AC}}{y_{Et}/x_{Et}} \#(3)$$

3.2. Calculation of activity coefficients from thermodynamic models

Three activity coefficient models are employed in this work, including semi-empirical models NRTL[23] and UNIQUAC[25] and predictive model UNIFAC[20].

Semi-empirical models. Non-Random Two-Liquid (NRTL) and Universal Quasi-Chemical (UNIQUAC) are local composition models based on the concept introduced by Wilson[22]. Both models are valid at low pressures (<1000 kPa) and well-adapted to ternary and

multicomponent mixtures involving highly diluted aroma compounds in hydroalcoholic mixtures[1].

NRTL has two sets of adjustable parameters, including A_{ij}^{0} and A_{ij}^{T}, which are fitted to experimental VLE data, and non-randomness parameter α_{ij}, which is set to 0.30 as recommended for systems containing water and polar non-associated substances[23].

In the UNIQUAC model, the combinatorial part is constituted by pure-component properties including coordination number Z, lattice parameter l_i, segment fraction Φ_i and area fractions θ_i and θ'_i. The residual term comprises two sets of binary interaction parameters that are determined from experimental VLE data. In this work, Z is set to 10 and the segment and area fractions of the studied system are calculated from pure-component constants (r_i, q_i and q'_i) whose values are listed in Table 3.

Table 3. Values of size and surface parameters[a] for α-terpineol, ethanol and water

Component	r_i	q_i	q'_i
α-terpineol	6.7897	5.2000	
ethanol	2.1055	1.9720	0.9600
water	0.9200	1.4000	1.0000

[a]Data made available in the Simulis Thermodynamics package (ProSim)[31]

Predictive methods. UNIFAC is a group-contribution tool based on the UNIQUAC equation[25] and on Wilson's solution-of-groups concept[47]. In the modified (Dortmund) version applied in this study, the residual term includes pure-component parameters q_i and r_i, which are calculated from the sum of group area parameters Q_k and group volume parameters R_k, respectively, whereas the group interaction parameter $\Psi_{n,m}$ is calculated from interaction parameters $a_{n.m}$, $b_{n.m}$ and $c_{n.m}$. Group decomposition for α-terpineol, ethanol and water, as well as Q_k, R_k and interaction parameters between the corresponding functional groups are listed in Tables 4 and 5.

Table 4. Modified UNIFAC (Dortmund) decomposition for α-terpineol, ethanol and water and volume and surface area parameters[a] for the different functional groups.

Group	Subgroup	α-terpineol	ethanol	water	*R*	*Q*
CH_2	CH_3	3	1		0.6325	1.0608
	CH_2		1		0.6325	0.7081
	C	1			0.6325	0.0000
C=C	CH=C	1			1.2832	0.8962
OH	OH(p)		1		1.2302	0.8927
	OH(t)	1			0.6895	0.8345
H_2O	H_2O			1	1.7334	2.4561
CY-CH_2	c-CH_2	3			0.7136	0.8635
	c-CH	1			0.3479	0.1071

[a]Data from the DDBST Dortmund Data Bank[48], made available in the Simulis Thermodynamics package (ProSim)[31].

Table 5. Modified UNIFAC (Dortmund) interaction parameters[a] between the subgroups in this study.

m	*n*	$a_{m,n}$	$b_{m,n}$	$c_{m,n}$	$a_{n,m}$	$b_{n,m}$	$c_{n,m}$	Ref
CH_2	C=C	189.66	-0.27232		-95.41801	0.061708		[49]
	OH	2777	-4.674	0.001551	1606	-4.746	0.0009181	[49]
	H_2O	1391.3	-3.6156	0.001144	-17.253	0.8389	0.0009021	[49]
	CY-CH_2	-117.1	0.5481	-0.00098	170.9	-0.8062	0.001291	[50]
C=C	OH	2649	-6.508	0.004822	1566	-5.809	0.005197	[49]
	H_2O	778.3	0.1482		-1301	4.072		[49]
	CY-CH_2	2.406	-0.1882		60.2	0.1565		[50]
OH	H_2O	-801.9	3.824	-0.007514	1460	-8.673	0.01641	[49]
	CY-CH_2	3121	-13.69	0.01446	2601	-1.25	-0.006309	[50]
H_2O	CY-CH_2	274.37	-0.5861	-0.00030011	1632.9	-2.8719	0.003455	[49]

[a]Data from the DDBST Dortmund Data Bank[48].

4. RESULTS AND DISCUSSION

This section is divided into two parts: (1) validation of the experimental methodology using the ebulliometer and the VLE results for α-terpineol highly diluted in ethanol-water mixtures; (2) correlation of the experimental data by semi-empirical thermodynamic models NRTL and UNIQUAC and predictions by the UNIFAC model.

4.1. Experimental VLE data

Validation of the apparatus and experimental protocol

The accuracy of the experimental device used for the VLE measurements and the suitability of the experimental protocol were validated by remeasuring the VLE of the binary system ethanol + water and applying thermodynamic consistency tests to the experimental data. This validation procedure can be extended to VLE measurements of our ternary mixtures due to the low concentrations of α-terpineol in the hydroalcoholic mixtures (in the order of 10^{-4} in mole fractions), which allow to infer that the thermodynamic behavior of the mixture is governed by the ethanol-water binary system[1,51]. This hypothesis was verified by plotting the densities at 25 °C measured for the liquid and vapor phases as a function of temperature for the binary system and comparing with those measured for the samples containing α-terpineol.

A total of 30 VLE points were measured for the binary ethanol-water. The experimental bubble and dew points are plotted in Figure 2 together with literature data[35,52] that are deemed consistent according to Jaubert et al.[53], and the corresponding VLE data are listed in Appendix B. Figure 2 also presents bubble and dew curves calculated using the NRTL model[23] with interaction parameters reported in previous works from our team[39,54]. These interaction parameters were adjusted to consistent, high-quality isothermal data measured by a static method[55,56]. As a result, the NRTL model is used here in a predictive way. As observed in the figure, the isobaric diagram obtained from our experimental points is in good agreement with the literature data and our experimental data are well described by the NRTL model with the parameters from Puentes et al. (2018)[54].

Indeed, the absolute average deviation for vapor composition ($|\Delta y_{Et}|$) was 0.007 in mole fraction, with a maximum value of 0.021 in the water-rich region of the phase diagram.

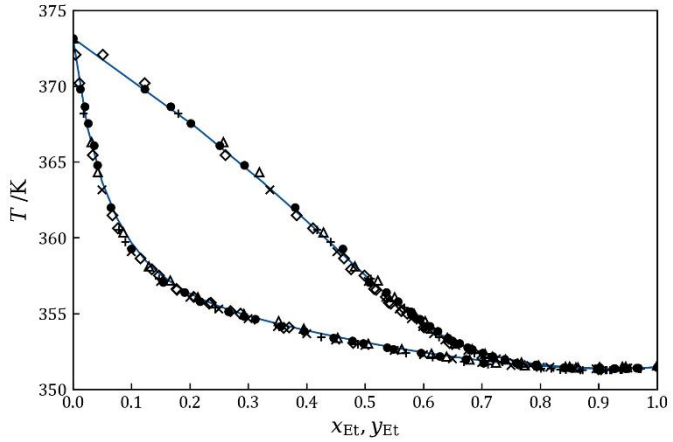

Figure 2. Isobaric phase diagram for the binary system ethanol (Et) + water (w) at 101.3 kPa. ●, experimental bubble and dew points; ◇, Hughes and Maloney[52]; ×, Kojima et al.[35]; +, Kamihama et al.[33]; Δ, Arce et al. [57]. The solid blue lines represent the bubble and dew curves calculated using the NRTL model with the parameters from Puentes et al. (2018)[54] listed in Table 8.

The different consistency tests employed for the binary data in this work and their respective results are thoroughly described in Appendix C. The binary VLE data measured in this work successfully passed the different tests.

Vapor-liquid equilibrium for α-terpineol highly diluted in hydroalcoholic mixtures

The vapor-liquid equilibrium at 101.3 kPa of the system highly diluted α-terpineol + ethanol + water was measured as described in section 2.2. The mole compositions of the liquid and vapor phases as determined by gas chromatography and density measurements are listed in Table 6.

Table 6. Experimental VLE data for the system highly diluted α-terpineol (αT) + ethanol (Et) + water (w) at P = 101.3 kPa[a,b]

T/K	ρ_L/g·cm^{-3}	ρ_{CV}/g·cm^{-3}	$x_{\alpha T}$	$u(x_{\alpha T})$	x_{Et}	$y_{\alpha T}$	$u(y_{\alpha T})$	y_{Et}
369.93	0.9922	0.9565	$4.10\cdot10^{-5}$	$0.07\cdot10^{-5}$	0.010	$83.95\cdot10^{-5}$	$1.25\cdot10^{-5}$	0.125
369.78	0.9918	0.9575	$4.56\cdot10^{-5}$	$0.08\cdot10^{-5}$	0.011	$103.20\cdot10^{-5}$	$1.55\cdot10^{-5}$	0.121
369.60	0.9915	0.9543	$4.78\cdot10^{-5}$	$0.08\cdot10^{-5}$	0.012	$112.38\cdot10^{-5}$	$1.66\cdot10^{-5}$	0.132
368.30	0.9894	0.9397	$6.74\cdot10^{-5}$	$0.12\cdot10^{-5}$	0.017	$104.12\cdot10^{-5}$	$1.45\cdot10^{-5}$	0.181
368.31	0.9889	0.9403	$6.28\cdot10^{-5}$	$0.11\cdot10^{-5}$	0.018	$92.50\cdot10^{-5}$	$1.29\cdot10^{-5}$	0.179
368.02	0.9885	0.9371	$6.74\cdot10^{-5}$	$0.12\cdot10^{-5}$	0.019	$94.20\cdot10^{-5}$	$1.30\cdot10^{-5}$	0.189
364.35	0.9798	0.8950	$7.61\cdot10^{-5}$	$0.13\cdot10^{-5}$	0.044	$58.86\cdot10^{-5}$	$0.69\cdot10^{-5}$	0.339
364.11	0.9799	0.8956	$8.57\cdot10^{-5}$	$0.14\cdot10^{-5}$	0.043	$67.97\cdot10^{-5}$	$0.80\cdot10^{-5}$	0.336
364.08	0.9801	0.8955	$8.96\cdot10^{-5}$	$0.15\cdot10^{-5}$	0.042	$68.97\cdot10^{-5}$	$0.81\cdot10^{-5}$	0.337
360.48	0.9673	0.8698	$9.95\cdot10^{-5}$	$0.16\cdot10^{-5}$	0.086	$27.34\cdot10^{-5}$	$0.29\cdot10^{-5}$	0.447
360.46	0.9701	0.8699	$9.54\cdot10^{-5}$	$0.15\cdot10^{-5}$	0.076	$24.58\cdot10^{-5}$	$0.26\cdot10^{-5}$	0.446
359.94	0.9690	0.8675	$9.80\cdot10^{-5}$	$0.16\cdot10^{-5}$	0.080	$22.40\cdot10^{-5}$	$0.23\cdot10^{-5}$	0.458
356.63	0.9490	0.8528	$10.72\cdot10^{-5}$	$0.16\cdot10^{-5}$	0.149	$8.02\cdot10^{-5}$	$0.08\cdot10^{-5}$	0.532
356.50	0.9423	0.8497	$10.72\cdot10^{-5}$	$0.15\cdot10^{-5}$	0.171	$5.82\cdot10^{-5}$	$0.06\cdot10^{-5}$	0.549
356.60	0.9423	0.8511	$10.48\cdot10^{-5}$	$0.15\cdot10^{-5}$	0.171	$5.95\cdot10^{-5}$	$0.06\cdot10^{-5}$	0.541
355.05	0.9097	0.8431	$12.83\cdot10^{-5}$	$0.16\cdot10^{-5}$	0.281	$4.31\cdot10^{-5}$	$0.04\cdot10^{-5}$	0.586
355.01	0.9073	0.8413	$12.43\cdot10^{-5}$	$0.15\cdot10^{-5}$	0.290	$4.20\cdot10^{-5}$	$0.04\cdot10^{-5}$	0.596
354.99	0.9092	0.8426	$12.86\cdot10^{-5}$	$0.16\cdot10^{-5}$	0.283	$4.15\cdot10^{-5}$	$0.04\cdot10^{-5}$	0.589

[a]Standard uncertainties are $u(T)$ = 0.2 K, $u(P)$ = 0.5 kPa, $u(\rho_L) = u(\rho_{CV})$ = 0.0002 g·cm^{-3}, $u(T_{\rho\_meas})$ = 0.03 K, $u(x_{Et}) = u(y_{Et})$ = 0.007. [b]T/K, equilibrium temperature; ρ/g·cm^{-3}, density of the liquid (L) and condensed vapor (CV) phases at 298.15 K; T_{ρ_meas}/K, temperature of the density measurement; **x** and **y,** mole compositions of the liquid and vapor phase, respectively.

Table 7 depicts the temperature dependency of pure component vapor pressure of α-terpineol ($P^0_{\alpha T}$ /kPa), along with its partition coefficients ($K_{\alpha T}$), relative volatilities ($\alpha_{\alpha T/Et}$) and infinite-dilution activity coefficients ($\gamma^{\infty}_{\alpha T}$). The different properties were calculated from the experimental VLE data using eqs 1-3. The experimental values for $K_{\alpha T}$ and $\alpha_{\alpha T/Et}$ as a function of ethanol mole composition are plotted in Figure 3.

The high values of the infinite dilution activity coefficient of α-terpineol ($\gamma^{\infty}_{\alpha T}$) depicted in Table 7 for the dilute region ($x_{Et} < 0.04$) are related to the high hydrophobicity of α-terpineol reported in Table 1 as log K_{ow} (2.98). This phenomenon has been reported in the literature for other hydrophobic aroma compounds such as long chain esters (isopentyl acetate, ethyl octanoate and ethyl decanoate), for which γ_i^{∞} is very large at high water content and decreases by several orders of magnitude when the proportion of ethanol is increased[27].

Table 7. Experimental VLE variables describing the behavior of α-terpineol (αT) highly diluted in hydroalcoholic mixtures at P = 101.3 kPa[a,b].

T/K	x_{Et}	$P^0_{\alpha T}$/kPa	$K_{\alpha T}$	K_{Et}	$\alpha_{\alpha T/Et}$	$\gamma^{\infty}_{\alpha T}$
369.93	0.010	1.08	20.46	12.03	1.70	1925.6
369.78	0.011	1.07	22.65	10.56	2.14	2148.9
369.60	0.012	1.06	23.51	10.95	2.15	2250.9
368.30	0.017	0.99	15.44	10.55	1.46	1582.8
368.31	0.018	0.99	14.72	9.81	1.50	1508.3
368.02	0.019	0.97	13.98	9.76	1.43	1454.5
364.35	0.044	0.80	7.73	7.77	1.00	979.4
364.11	0.043	0.79	7.93	7.76	1.02	1017.0
364.08	0.042	0.79	7.70	7.92	0.97	989.3
360.48	0.086	0.65	2.75	5.22	0.53	430.2
360.46	0.076	0.65	2.58	5.87	0.44	403.8
359.94	0.080	0.63	2.29	5.74	0.40	368.8
356.63	0.149	0.52	0.75	3.57	0.21	145.4
356.50	0.171	0.52	0.54	3.20	0.17	106.3
356.60	0.171	0.52	0.57	3.16	0.18	110.5
355.05	0.281	0.48	0.34	2.08	0.16	71.6
355.01	0.290	0.47	0.34	2.05	0.16	72.1
354.99	0.283	0.47	0.32	2.08	0.16	68.9

[a]Standard uncertainties are $u(T)$ = 0.2 K, $u(P)$ = 0.5 kPa, $u(x_{Et})$ = 0.007. [b]T/K, equilibrium temperature; x_{Et}, ethanol mole fractions in the liquid phase; $P^0_{\alpha T}$ /kPa, vapor pressure calculated with eq 1; $K_{\alpha T}$ and K_{Et}, partition coefficient of α-terpineol and ethanol, respectively; $\alpha_{\alpha T/Et}$, relative volatility of α-terpineol in relation to ethanol; $\gamma^{\infty}_{\alpha T}$, infinite dilution activity coefficient of α-terpineol.

As observed in Figures 3a and 3b, the absolute volatilities of α-terpineol in the hydroalcoholic mixtures are lower than 1 for ethanol mole fractions above 0.15, a region at which the aroma compound is more concentrated in the liquid phase. In the water-rich region (x_{Et} < 0.15), $K_{\alpha T}$ increases exponentially, and the compound can be up to 30 times more abundant in the vapor phase. Inversely, in the ethanol-rich region (x_{Et} > 0.50), α-terpineol concentration can be over 10 times higher in the liquid phase ($K_{\alpha T}$ < 0.1). As per the relative volatility, Figures 3c and 3d show that α-terpineol is more volatile than ethanol only for ethanol mole fractions below 0.04.

A similar behavior has been observed in other studies for the VLE of aroma compounds highly diluted in ethanol-water mixtures[27,28,39,58,59] and is mainly associated with two

factors: (1) the decrease in equilibrium temperature with consequent decrease of pure component vapor pressures[60,61] and (2) the increase in solubility of aroma compounds with increasing ethanol concentration due to a reduction in the free energy of the mixture[62]. The latter phenomenon is well correlated with the high log K_{ow} value (i.e. high hydrophobicity) of α-terpineol reported in Table 1. Another factor potentially driving the accentuated decrease in volatility observed for α-terpineol until $x_{Et} < 0.25$ is the change in molecular structure of the hydroalcoholic solution. In aqueous solutions containing small amounts of ethanol ($x_{Et} < 0.05$), alcohol molecules are monodispersed in the matrix. Increasing ethanol mole concentration up to about $x_{Et} = 0.25$ results in progressive aggregation of ethanol molecules and the formation of pseudo-micelles, which are liable to entrap hydrophobic aroma molecules, thus hampering their release into the vapor phase. Once a second critical value is reached with ethanol concentrations above $x_{Et} \approx 0.25$ the aggregates dissociate and water becomes monodispersed in the ethanolic solution instead[62–65]. However, had α-terpineol been incorporated into ethanol pseudo-micelles, an increase in the volatility of the terpene would be expected once ethanol concentration in the mixtures surpassed the second critical point, which is not the case in this study.

Repeatability of VLE assays was lower in the more aqueous region, where the volatility of α-terpineol is more pronounced and slight variations in temperature between experimental runs are likely to result in large differences in composition between the three independent runs. Temperature fluctuations are passible of occurring in dynamic ebulliometers operating at low pressures due to an overheating of the liquid in the boiling chamber[66], a phenomenon that is more accentuated in the aqueous region.

4.2. Thermodynamic modeling and validation

The experimental VLE data for the system highly diluted α-terpineol + ethanol + water at 101.3 kPa were correlated using semi-empirical models NRTL and UNIQUAC. The results were compared to those obtained from the predictive method UNIFAC. The ideal gas law was used to model the vapor phase, whereas for the liquid phase activity coefficients were calculated by fitting the experimental data to the excess Gibbs energy models using the software Simulis Thermodynamics (v. 2.0.34, ProSim)[31].

For the NRTL model, the non-randomness parameter α_{ij} was fixed at 0.30, as recommended in the literature for VLE of mixtures of polar liquids such as hydroalcoholic mixtures[23]. For the sub-systems α-terpineol (1) + ethanol (2) and α-terpineol (1) + water (3), the temperature-dependent parameters A_{ij}^{T}/J·mol^{-1}·K^{-1} and A_{ji}^{T}/J·mol^{-1}·K^{-1} are set to zero, since the influence of the highly diluted α-terpineol on the equilibrium temperature is deemed negligible [1,51] and the influence of temperature on measurements is incorporated in the variations in boiling temperatures as a function of ethanol composition. As per the binary sub-system ethanol (2) + water (3), the major compounds governing thermal equilibrium, binary interaction parameters were set to values from the literature[54] reported in Table 8, and parameters A_{ij}^{T}/J·mol^{-1}·K^{-1} and A_{ji}^{T}/J·mol^{-1}·K^{-1} are taken into consideration. These ethanol-water interaction parameters have been consistently used by our team for all systems aroma compound + ethanol + water for the simulation of spirit distillation processes. They were thus not fitted to our experimental data.

Given these considerations, the correlation of the experimental data for the system α-terpineol (1) + ethanol (2) + water (3) with NRTL and UNIQUAC models is narrowed down to a regression of four binary interaction parameters: A_{12}^{0}/J·mol^{-1} and A_{21}^{0}/J·mol^{-1}, for the binary α-terpineol (1) + ethanol (2); A_{13}^{0}/J·mol^{-1} and A_{31}^{0}/J·mol^{-1}, for the binary α-terpineol (1) + water (3). The parameters were estimated through the Microsoft Excel Solver add-in by minimizing the objective function for the partition coefficient of α-terpineol, $K_{\alpha T}$:

$$OF = \sum_{i=1}^{N} \left(\frac{K_{i\alpha T_{exp}} - K_{i\alpha T_{calc}}}{K_{i\alpha T_{exp}}} \right)^2 \#(4)$$

in which $K_{\alpha T_{exp}}$ is the experimental partition coefficient calculated from eq 2 and $K_{\alpha T_{calc}}$ is the partition coefficient calculated with the thermodynamic models. The calculation of $K_{\alpha T_{calc}}$was performed using the bubble temperature algorithm of the software Simulis Thermodynamics, which computes saturated liquid temperature (T) and vapor phase composition (**y**) at equilibrium from experimental pressure (P) and liquid phase composition (**x**).

The binary interaction parameters obtained for the two semi-empirical models are listed in Table 8. They were used to obtain values for $K_{\alpha T}$, $\alpha_{\alpha T/Et}$, $\gamma_{\alpha T}^{\infty}$ and g^E/RT for the entire composition range, which were then plotted with the experimental data. Figure 3 depicts the evolution of the partition coefficient (3a) and the relative volatility (3c) of α-terpineol as a function of ethanol mole composition in the liquid phase. A closeup view of the two figures is presented in Figures 3b and 3d to increase visibility of the data in the region of lower volatility.

Table 8. Binary interaction parameters for the system highly diluted α-terpineol (1) + ethanol (2) + water (3) from experimental data fitted by NRTL and UNIQUAC models to minimize the objective function (eq 4).

Model	Binary (i-j)	A_{ij}^0/J·mol^{-1}	A_{ij}^0/J·mol^{-1}	A_{ij}^T/J·mol^{-1}·K^{-1}	A_{ij}^T/J·mol^{-1}·K^{-1}	α_{ij}	Source
NRTL	(1)-(2)	22892.471	6915.164	0	0	0.3	a
	(1)-(3)	-1217.327	25981.358	0	0	0.3	a
	(2)-(3)	142.44	3559.28	-7.53	23.63	0.3	b
UNIQUAC	(1)-(2)	0.000	1782.494	0	0		a
	(1)-(3)	4785.484	0.000	0	0		a
	(2)-(3)	6060.98	-6293.61	-16.74	20.90		c

[a]this work. [b]Puentes et al., 2018[54]. [c]Delgado et al, 2007[67]

A good agreement was found between the NRTL model and the experimental data, with slight discrepancies for $\alpha_{\alpha T/Et}$ at ethanol mole fractions below 0.1 (Figure 3c). The UNIQUAC model underestimates both $K_{\alpha T}$ and $\alpha_{\alpha T/Et}$ in the region below 0.05 and above 0.25 ethanol mole fraction and thus fails to fit experimental data in the region nearing pure water. Since in spirit distillation the region of interest is specifically that of low ethanol concentration, UNIQUAC might not be well suited to explain the behavior of α-terpineol during distillation, in which case NRTL would be a more adequate model choice.

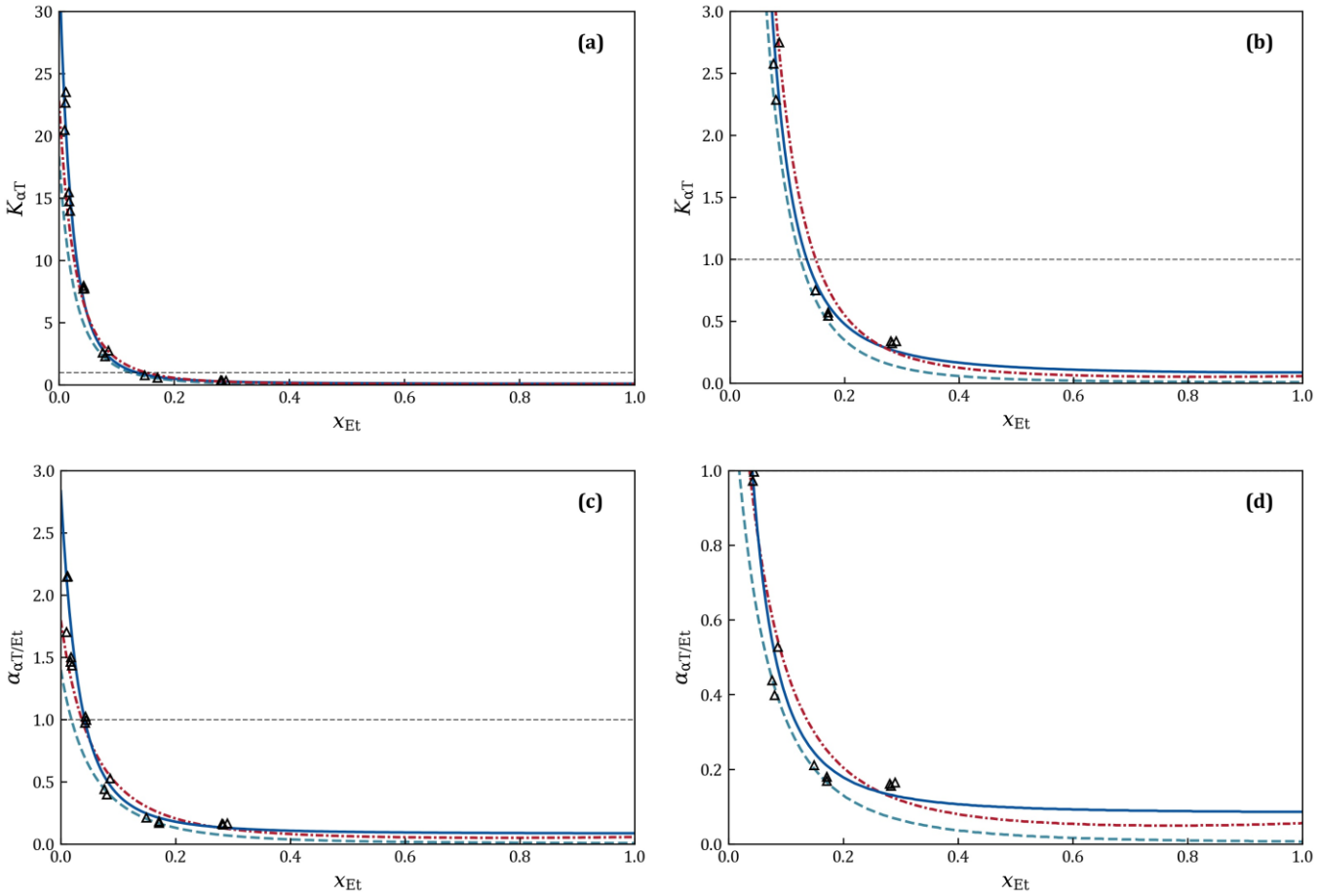

Figure 3. Evolution of (a, b) the partition coefficient ($K_{\alpha T}$) and (c,d) the relative volatility of α-terpineol ($\alpha_{\alpha T/Et}$) with ethanol mole fraction in the liquid phase (x_{Et}): Δ, experimental data from this work; —— (solid blue line), NRTL model; -·-·- (dash-dot red line), UNIQUAC model; - - - (dashed green line), UNIFAC prediction.

For comparative purposes, VLE data for the system was additionally predicted by the modified UNIFAC (Dortmund) model, with the structural and interaction parameters listed in Tables 4 and 5. As illustrated in Figure 3, values of absolute and relative volatility predicted by the UNIFAC model are lower than the experimental values for the entire ethanol composition range. Although the behavior of α-terpineol predicted by the model follows the same tendencies as that from the experimental data, the model was unable to accurately predict VLE data for the system studied. Since group interaction parameters used in the UNIFAC model derive from a reduction of binary experimental data over a large composition range, it is not surprising that the model is not adapted for highly diluted compounds as is the case in this work.

The evolution of the infinite dilution activity coefficient of α-terpineol ($\gamma_{\alpha T}^{\infty}$) as a function of temperature and ethanol composition is depicted in Figure 4. The increase in values of $\gamma_{\alpha T}^{\infty}$ with temperature or decreasing ethanol concentration indicate that the non-ideality of the liquid phase is more pronounced in more dilute regions, where hydrogen bonding between water molecules is stronger and partial pressure of α-terpineol is lower, as discussed in subsection 4.1. Such marked variations in activity coefficients at lower ethanol mole fractions make experimental VLE measurements quite challenging, increasing the chance of imprecisions[19]. Figure 4 highlights that NRTL was the best suited model amongst the three models tested to adequately represent the evolution of the activity coefficient with temperature and ethanol composition, followed by UNIQUAC. Once again, UNIFAC provides underestimated predictions over the entire composition range.

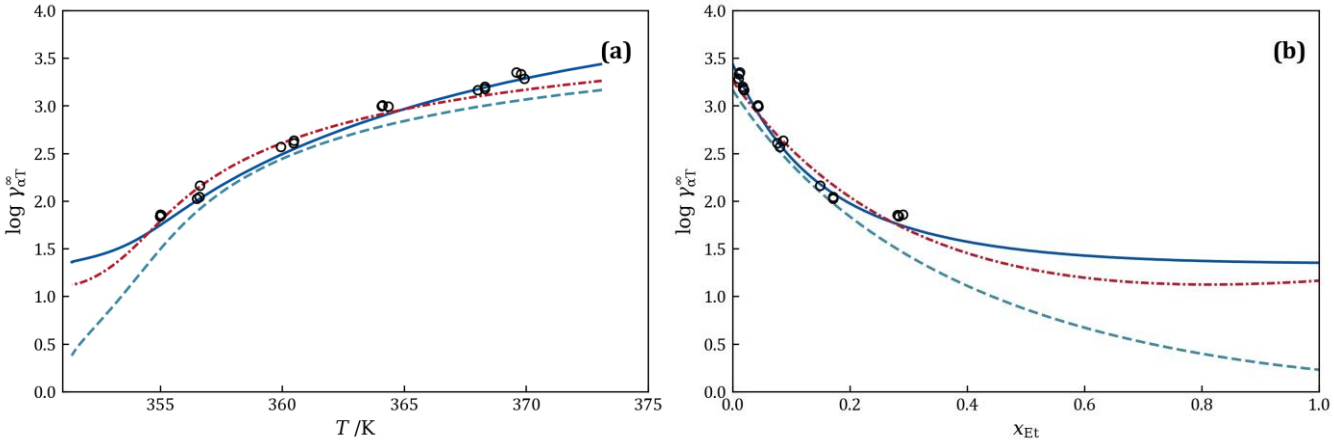

Figure 4. Evolution of log of infinite dilution activity coefficient of α-terpineol ($\log \gamma_{\alpha T}^{\infty}$) with (a) temperature and with (b) ethanol mole fraction (x_{Et}). o, experimental data from this work; —— (solid blue line), NRTL model; -·-·- (dash-dot red line), UNIQUAC model; - - - (dashed green line), UNIFAC prediction.

The fitting quality of the thermodynamic models was evaluated by the root-mean-square deviation (RMSD) and the average absolute relative deviation (AAD%) according to eqs 5-6, in which N is the number of experimental points and E is equilibrium variable $K_{\alpha T}$, $\alpha_{\alpha T/Et}$ or $\gamma_{\alpha T}^{\infty}$. The data calculated from NRTL, UNIQUAC and UNIFAC are reported in Table 9. The residual values are higher than the tolerance stipulated in the literature[68], especially for UNIQUAC and UNIFAC. Nonetheless, given the difficulties to accurately measure and quantify highly diluted compounds, the RMSD and AAD% values for the NRTL model

remain acceptable. The relative deviations between the experimental data and the values calculated with the different models for $K_{\alpha T}$ are presented in Figure 5.

$$RMSD = \left[\frac{1}{N}\sum_{i=1}^{N}\left(E_{\alpha T i_{exp}} - E_{\alpha T i_{calc}}\right)^2\right]^{\frac{1}{2}} \#(5)$$

$$AAD\% = \frac{1}{N}\sum_{i=1}^{N}\left|\frac{E_{\alpha T i_{exp}} - E_{\alpha T i_{calc}}}{E_{\alpha T i_{exp}}}\right| 100\% \#(6)$$

Table 9. Fitting quality statistics[a] for NRTL, UNIQUAC and UNIFAC models for the system highly diluted α-terpineol + ethanol + water.

		NRTL	UNIQUAC	UNIFAC
$K_{\alpha T}$	RMSD	1.1	2.9	4.6
	AAD%	12.9%	23.5%	35.3%
$\alpha_{\alpha T/Et}$	RMSD	0.2	0.2	0.4
	AAD%	15.1%	23.3%	31.8%
$\gamma_{\alpha T}^{\infty}$	RMSD	116.0	286.3	463.0
	AAD%	11.8%	22.6%	36.2%

[a] $K_{\alpha T}$, partition coefficient of α-terpineol; $\alpha_{\alpha T/Et}$, relative volatility of α-terpineol in relation to ethanol; $\gamma_{\alpha T}^{\infty}$, infinite dilution activity coefficient of α-terpineol; RMSD, root-mean-square deviation; AAD%, average absolute relative deviation.

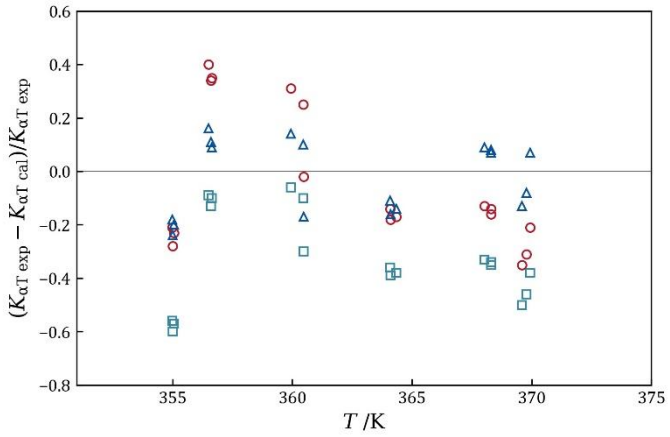

Figure 5. Relative deviations of experimental partition coefficients ($K_{\alpha T\,exp}$) from values calculated using the different models ($K_{\alpha T\,cal}$) for alpha-terpineol highly diluted in ethanol + water mixtures. △,NRTL; ○,UNIQUAC; □,UNIFAC.

The results show that the semi-empirical models fitted to experimental data are better adapted than the group-contribution predictive method for the VLE of the system highly diluted α-terpineol + ethanol + water at atmospheric pressure. Similar results have been observed in other studies for systems consisting of aroma compounds highly diluted in hydroalcoholic mixtures[14,69].

5. CONCLUSIONS

Vapor-liquid equilibrium of the system highly diluted α-terpineol + ethanol + water at 101.3 kPa has been measured from (354.99 to 369.93) K. Results show that α-terpineol is more volatile than ethanol in highly dilute regions with ethanol mole fractions below 0.04, its volatility decreasing when ethanol concentration in the liquid phase is increased. The experimental data was modeled using two semi-empirical models, NRTL and UNIQUAC, and compared to the data predicted by the UNIFAC model. The NRTL model provided the best correlation for the system, with average relative deviations of 12.9 and 11.8% for $K_{\alpha T}$ and
$\gamma_{\alpha T}^{\infty}$, respectively. The binary interaction parameters obtained in this work will prove useful to represent the behavior of aroma compounds in distillation processes for alcoholic beverages using computer simulation models.

APPENDIX A. Verification of the density measurements and the relationship between density and ethanol concentration of hydroalcoholic solutions

The accuracy of the density measurements was verified by comparing experimental measurements for ethanol-water mixtures of known composition with data from the literature (Figure A-1). The mixtures were prepared by weight using a precision scale with a resolution of ± 0.0001 g. To limit evaporation during mixture preparation, both compounds were kept at low temperatures and the least volatile compound was weighed first. The experimental composition and density measurements at 298.15 K and atmospheric pressure for nineteen mixtures are listed in Table A-1. Furthermore, Figure A-2 depicts a parity plot between the ethanol mole fractions from the weighed values and those calculated from density using the mathematical model from Wagenbreth and Blanke[43], as described in subsection 2.3. A good correspondence is observed between the two values, with average absolute and relative deviations of 0.0006 and 0.5%, respectively.

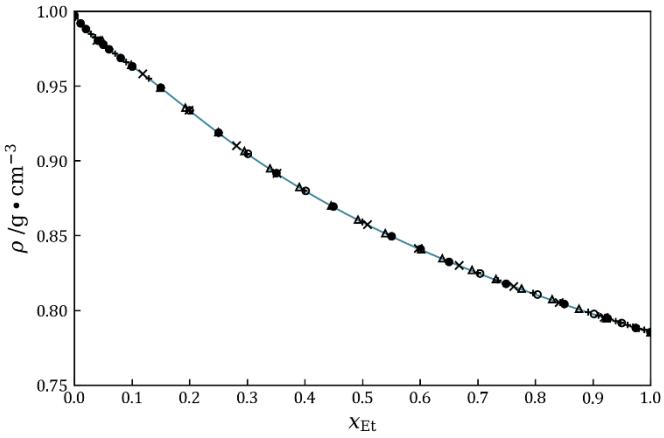

Figure A-1. Density measurements for ethanol-water mixtures as a function of ethanol mole fraction (x_{Et}) at T = 298.15 K and atmospheric pressure. ●, this work; Δ, Arce et al. [70]; +, Hoga et al. [71]; ×, Zarei et al. [72]; ○, González et al. [73]. The solid green line represents the evolution of density with ethanol composition from the OIML alcoholometric tables [44].

Table A-1. Density measurements at 298.15 K and atmospheric pressure (P = 0.1 MPa) and experimental ($x_{Et\ exp}$) ethanol mole fractions for ethanol-water mixtures of known compositions[a].

$x_{Et\ exp}$	ρ/g.cm^{-3}
0.0000	0.9971
0.0107	0.9920
0.0200	0.9880
0.0409	0.9805
0.0502	0.9776
0.0601	0.9747
0.0801	0.9687
0.1002	0.9630
0.1501	0.9488
0.2500	0.9187
0.3507	0.8917
0.4494	0.8693
0.5504	0.8496
0.6500	0.8325
0.7491	0.8179
0.8502	0.8042
0.9252	0.7947
0.9744	0.7884
1.0000	0.7854

[a]Standard uncertainties are $u(x_{Et\ exp})$ = 0.0001, $u(\rho)$ = 0.0002 g·cm^{-3} and $u(T_{\rho\_meas})$ = 0.03 K.

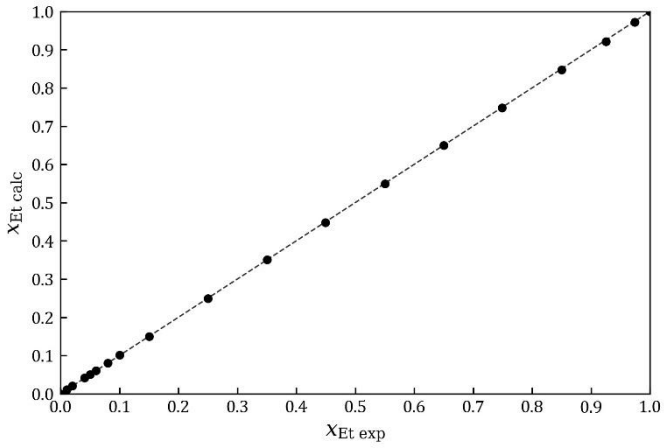

Figure A-2. Parity plot for ethanol mole fraction of ethanol-water mixtures determined experimentally ($x_{Et\ exp}$) and calculated from density ($x_{Et\ calc}$) at T = 298.15 K and atmospheric pressure.

APPENDIX B. Phase behavior study of the binary system ethanol + water

Table B-1 reports experimental VLE data of T, x_{Et} and y_{Et} for the binary system ethanol + water at P = 101.3 kPa, in addition to the calculated activity coefficients and the excess Gibbs function in its dimensionless form. The non-ideality of the vapor phase was neglected, and activity coefficients and excess Gibbs energy (g^E) were calculated for the liquid phase. The values reported for temperature and composition comprise all significant digits measured, even if those are greater than the uncertainties associated with the measurements. This choice was made considering the azeotropic region of the binary system, in which the bubble and dew curves are nearly flattened-out and the temperature range is extremely narrow. Despite the experimental uncertainty, the reported values around the azeotrope are logical in that they follow the expected trend, the ethanol mole fraction in the liquid phase being slightly superior to that in the vapor phase for the three points measured between the azeotrope and pure ethanol (at $x_{Et} > 0.9$).

The azeotropic point of the system at 101.3 kPa can be estimated using our experimental data and a simple graphical method. The azeotropic point was found to be at $x_{Et\ az} \approx 0.905$, in mole fraction, and $T_{az} \approx 351.37$ K (78.22 °C). These values are in good agreement with previously reported azeotropic data, which range from $x_{Et\ az}$ = (0.893 to 0.905) and T_{az} = (351.25 to 351.45) K [36,55].

Table B-1. Experimental isobaric VLE data at 101.3 kPa for the binary system ethanol (Et) + water (w)[a].

T/K	ρ_L/g·cm^{-3}	ρ_{CV}/g·cm^{-3}	x_{Et}	y_{Et}	γ_{Et}	γ_w	g^E/RT
373.15	0.9971		0.0000	0.0000		1.000	0.000
369.80	0.9912	0.9567	0.0128	0.1231	4.867	1.003	0.023
368.66	0.9881	0.9435	0.0202	0.1672	4.366	1.000	0.030
367.54	0.9859	0.9329	0.0261	0.2019	4.236	1.005	0.043
366.07	0.9824	0.9183	0.0358	0.2510	4.056	1.006	0.056
364.79	0.9803	0.9063	0.0420	0.2938	4.237	1.001	0.062
362.00	0.9732	0.8844	0.0651	0.3805	3.912	1.001	0.089
359.27	0.9633	0.8664	0.0999	0.4619	3.425	1.003	0.126
357.06	0.9474	0.8574	0.1542	0.5071	2.649	1.066	0.204
356.39	0.9363	0.8519	0.1909	0.5365	2.322	1.076	0.220
355.78	0.9283	0.8483	0.2173	0.5566	2.165	1.090	0.236
355.12	0.9140	0.8445	0.2660	0.5778	1.883	1.136	0.262
354.81	0.9066	0.8435	0.2925	0.5835	1.751	1.177	0.279
354.62	0.9014	0.8418	0.3120	0.5937	1.682	1.190	0.282
354.16	0.8903	0.8388	0.3557	0.6112	1.546	1.239	0.293
353.83	0.8807	0.8366	0.3963	0.6246	1.437	1.294	0.299
353.40	0.8697	0.8338	0.4465	0.6422	1.333	1.369	0.302
353.20	0.8631	0.8326	0.4783	0.6497	1.269	1.433	0.302
353.03	0.8594	0.8307	0.4968	0.6616	1.252	1.445	0.297
352.74	0.8516	0.8286	0.5381	0.6757	1.194	1.527	0.291
352.65	0.8496	0.8274	0.5489	0.6834	1.188	1.532	0.287
352.39	0.8414	0.8247	0.5960	0.7010	1.134	1.633	0.273
352.18	0.8361	0.8221	0.6282	0.7186	1.112	1.684	0.260
351.97	0.8290	0.8191	0.6730	0.7395	1.077	1.788	0.240
351.73	0.8245	0.8163	0.7026	0.7591	1.069	1.836	0.227
351.62	0.8158	0.8115	0.7627	0.7937	1.034	1.978	0.187
351.42	0.8051	0.8038	0.8407	0.8504	1.013	2.156	0.133
351.37	0.7977	0.7976	0.8977	0.8984	1.004	2.285	0.088
351.37	0.7939	0.7941	0.9281	0.9263	1.001	2.359	0.063
351.38	0.7912	0.7916	0.9494	0.9458	0.999	2.464	0.045
351.41	0.7889	0.7893	0.9682	0.9650	0.998	2.526	0.028
351.45	0.7854		1.0000	1.0000	1.000		0.000

[a]Standard uncertainties are $u(T)$ = 0.2 K, $u(P)$ = 0.5 kPa, $u(\rho_L) = u(\rho_{CV})$ = 0.0002 g·cm^{-3}, $u(T_{\rho\_meas})$ = 0.03 K, and $u(x_{Et}) = u(y_{Et})$ = 0.007. [b]T/K, equilibrium temperature; ρ/g·cm^{-3}, density of the liquid (L) and condensed vapor (CV) phases at 298.15 K; T_{ρ_meas}/K, temperature of the density measurement; x_{Et}, liquid phase ethanol mole fraction; y_{Et}, vapor phase ethanol mole fraction; γ_i, activity coefficient of component i; g^E/RT, Gibbs dimensionless function.

Figure B-1 presents the activity coefficients and g^E/RT obtained from the experimental data as a function of the mixture composition. Activity coefficients and g^E/RT data for the same system from Kamihama et al. [33] and Arce et al.[57] have been added for comparison.

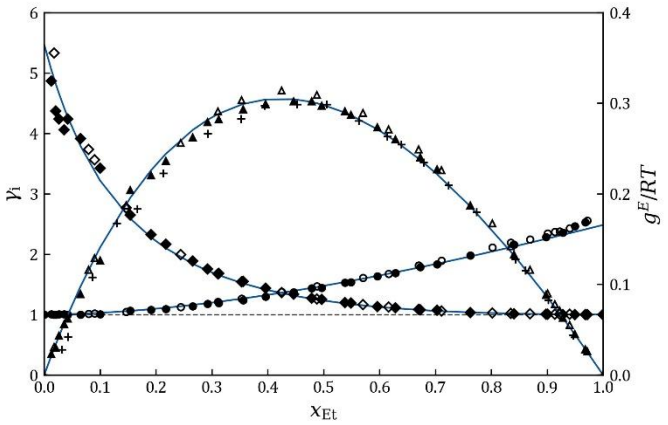

Figure B-1. Plot of the experimental activity coefficients and excess Gibbs energy as a function of ethanol mole fraction for the binary system ethanol (Et) + water (w) at 101.3 kPa. ◆, experimental γ_{Et}; ◇, γ_{Et} from Kamihama et al.[33]; ●, experimental γ_w; ○, γ_w from Kamihama et al.[33]; ▲, g^E/RT from this work; Δ, g^E/RT from Kamihama et al.[33]; +, g^E/RT from Arce et al.[57]. The solid blue lines represent the curves calculated using the NRTL model with the parameters from Puentes et al. (2018)[54] listed in Table 8.

The expanded combined uncertainty associated with the determination of ethanol composition from density measurements was calculated according to the law of propagation of uncertainty and is estimated to be ±0.015 (k=2). Sources of uncertainty used for the calculation and their respective estimates and probability distributions are listed in Table B-2.

Table B-2. Standard uncertainties used for estimating the combined uncertainty related to the determination of ethanol composition from density measurements.

Source of uncertainty	Estimate	Distribution
Density ($g \cdot cm^{-3}$)	0.0002	rectangular
Repeatability of density	0.00006	gaussian
Temperature (K)	0.03	rectangular
Density equation	0.0003	gaussian
Ethanol purity	0.001	rectangular

APPENDIX C. Thermodynamic consistency of the measured VLE data for the binary system ethanol (Et) + water (w)

In order to validate our apparatus and the experimental method employed for the measurements, consistency tests were performed on the experimental binary VLE data using

three different tests: the Redlich-Kister area test[74], as described by Wisniak et al.[75], the Van Ness[76] point test modified by Fredenslund[77] and the Wisniak test (also called the L-W test)[78] combining a point test and an area test.

Redlich-Kister area test [74]

The Redlich-Kister test is based on the Gibbs-Duhem equation. For experimental data measured under isobaric conditions, the following equality can be written:

$$\int_{x_{\mathrm{Et}}=0}^{x_{\mathrm{Et}}=1} \ln\frac{\gamma_{\mathrm{Et}}}{\gamma_{\mathrm{w}}}\mathrm{d}x_{\mathrm{Et}} = \int_{T(x_{\mathrm{Et}}=0)}^{T(x_{\mathrm{Et}}=1)} \frac{h^E}{RT^2}\mathrm{d}T \ \#(\mathrm{C1})$$

where h^E is the excess enthalpy of the mixture at the bubble point. The right-hand side of eq C1 was estimated using an empirical correlation proposed by Larkin[79] and based on his experimental measurements. The estimated numerical value was found to be very small and thus can be neglected.

When $\ln(\gamma_{\mathrm{Et}}/\gamma_{\mathrm{w}})$ is plotted against x_{Et}, the areas A+ and A- between the resulting curve and the x-axis must be the same (Figure C-1). Theoretically, perfect data would result in A+ = A-. In practice, however, experimental errors are inevitable, whether from systematic errors from the instruments, from the presence of impurities in the chemical components used or from manipulation errors. In light of this, experimental data is evaluated according to eq C2 and can be declared consistent if $D < 2$[75].

$$D = 100\frac{|A^+ - A^-|}{A^+ + A^-} \#(\mathrm{C2})$$

In our case, experimental data successfully passed the area test with D ≈ 1.23.

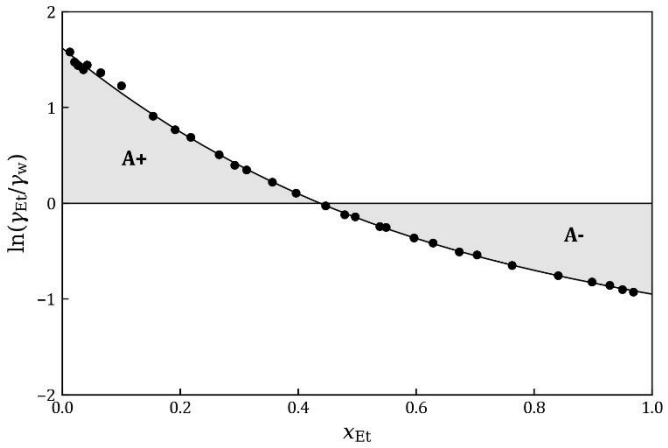

Figure C-1. Redlich-Kister consistency test for the binary system ethanol (Et) + water (w) at 101.3 kPa. ●, experimental data from this work.

Fredenslund's test (point test)[77]

The Van Ness test[76] described by Fredenslund et al.[77] and Gmehling et al.[80] has also been used to test the consistency of the data. The test is described in depth in several works in the literature, being often referred to as the point-to-point test. Briefly, according to the phase rule, for a binary system at VLE variance equals 2. The principle of the test is thus to use only two variables of the reported data (e.g. T and $x_{\mathrm{Et\,exp}}$) to calculate the third one (y_{Et}).

From the fitted parameters, it is possible to calculate the activity coefficients and finally the vapor phase compositions ($y_{\mathrm{i\,calc}}$), given that the experimental values of y_i were not used for fitting the parameters. Experimental values ln γ_{Et}, ln γ_{w}, and $g^E/(RTx_{\mathrm{Et}}x_{\mathrm{w}})$ plotted against x_{Et} are shown in Figure C-2, along with pertinent curves calculated using a Legendre polynomial with five coefficients fitted to the experimental data.

To do so, $(g^E/RT)_{\mathrm{exp}}$ data are used to fit the parameters of a Redlich-Kister equation or a series of Legendre polynomials.

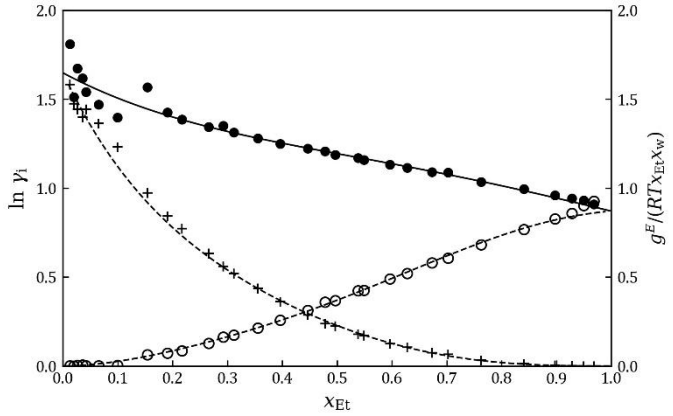

Figure C-2. Activity coefficient-composition relationships for the consistency test of Fredenslund[77]. +, experimental ln γ_{Et}; ○, experimental ln γ_w; ●, experimental $g^E/(RTx_{Et}x_w)$. Solid and dashed lines represent the calculated curves by using Legendre polynomials.

A set of n data points is considered thermodynamically consistent by the point-to-point test [77,80] if:

$$\sum_{i=1}^{n} \frac{|y_{i\,exp} - y_{i\,cal}|}{n} \leq 0.01 \#(\mathrm{C3})$$

A value of 0.0061 is obtained for our data, suggesting that the data are consistent. However, when the residuals in mole fraction are considered, larger values are obtained for the experimental points at small ethanol concentrations. Moreover, in the same dilute region of the system, there is a slight lack of randomness in the distribution of the residuals of vapor phase composition. Such observations are common for this kind of phase diagram[81]. Indeed, in this dilute region of the phase diagram (small ethanol mole fraction) the slope of the bubble curve is very high, so that a small error in experimental composition (or in the effective pressure of the experimental device) is likely to entail a large error in temperature.

The L-W test of Wisniak[78]

The thermodynamic consistency of our data was additionally evaluated using the L-W test developed by Wisniak[78], which is now routinely employed by many authors[82–84]. The test can be described by the following expressions:

$$L_i = \frac{\sum T_i^0 x_i \Delta s_i^0}{\sum x_i \Delta s_i^0} - T = \frac{g^E}{\sum x_i \Delta s_i^0} - \frac{RT}{\sum x_i \Delta s_i^0} \sum x_i \ln \frac{y_i}{x_i} = W_i \#(C4)$$

in which, for a pure component i, T_i^0/K is the boiling temperature, Δs_i^0/J·K^{-1} is the entropy of vaporization, with $\Delta s_i^0 = \Delta h_i^0 / T_i^0$, and Δh_i^0/J is the vaporization enthalpy. The values of Δh_{Et}^0 and Δh_w^0 used in this work originate from Poling et al.[85].

An experimental point passes the test if:

$$0.92 < L_i/W_i < 1.08 \#(C5)$$

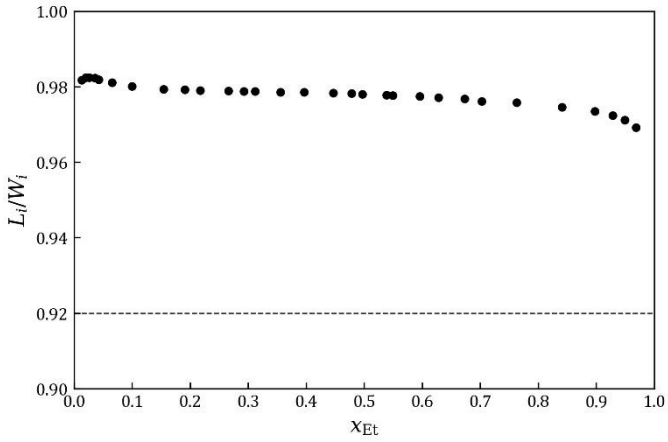

Figure C-3. Application of the Wisniak test to the experimental points.

Figure C-3 indicates that our experimental data pass the Wisniak test, as confirmed by the resulting value of $0.969 < L_i/W_i < 0.982$.

For binary systems, the test can also be employed as an area test with:

$$L = \int_0^1 L_i \, dx_1 \quad (C6); \qquad W = \int_0^1 W_i \, dx_1 \quad (C7) \quad \text{and} \quad D = 100 \, \frac{|L - W|}{L + W} \#(C8)$$

Experimental data are declared consistent if $D < 3$[75].

Our experimental data resulted in D = 1.10, with L = 7.81 and W = 7.99.

Results obtained using the different consistency tests described above evidence that the VLE data measured in this work are thermodynamically consistent.

AUTHOR INFORMATION

Corresponding author

*Gabriela Zanghelini. E-mail: gabriela.zanghelini@agroparistech.fr

ORCID

Gabriela Zanghelini: 0000-0001-6993-3878

Violaine Athès: 0000-0002-2194-8517

Martine Esteban-Decloux: 0000-0002-8084-2528

Pierre Giampaoli: 0000-0002-6756-0403

Stéphane Vitu: 0000-0002-5442-1279

Notes

The authors declare no competing financial interest.

Funding

This work was supported by the foundation Jean Poupelain.

Acknowledgements

The authors are thankful to Nicolas Descharles for the valuable assistance with the analytical measurements.

REFERENCES

[1] J.O. Valderrama, C.A. Faúndez, L.A. Toselli, Advances on modeling and simulation of alcoholic distillation. Part 1: Thermodynamic modeling, Food Bioprod. Process. 90 (2012) 819–831. https://doi.org/10.1016/j.fbp.2012.04.004.

[2] A. Ammari, K. Schroen, Flavor Retention and Release from Beverages: A Kinetic and Thermodynamic Perspective, J. Agric. Food Chem. 66 (2018) 9869–9881. https://doi.org/10.1021/acs.jafc.8b04459.

[3] L. Paravisini, E. Guichard, Interactions between aroma compounds and food matrix, Flavour From Food to Percept. (2016) 208–234. https://doi.org/10.1002/9781118929384.ch9.

[4] J. Marais, Terpenes in the Aroma of Grapes and Wines: A Review, South African J. Enol. Vitic. 4 (1983) 49–58. https://doi.org/10.21548/4-2-2370.

[5] Y.Z. Gunata, C.L. Bayonove, R.L. Baumes, R.E. Cordonnier, The aroma of grapes I. Extraction and determination of free and glycosidically bound fractions of some grape aroma components, J. Chromatogr. A. 331 (1985) 83–90. https://doi.org/10.1016/0021-9673(85)80009-1.

[6] R. Cantagrel, L. Lurton, J.P. Vidal, B. Galy, From vine to Cognac, in: Fermented Beverage Prod., 1995: pp. 208–228. https://doi.org/10.1007/978-1-4757-5214-4_8.

[7] J.C. Amorim, R.F. Schwan, W.F. Duarte, Sugar cane spirit (cachaça): Effects of mixed inoculum of yeasts on the sensory and chemical characteristics, Food Res. Int. 85 (2016) 76–83. https://doi.org/10.1016/j.foodres.2016.04.014.

[8] J. Cacho, L. Moncayo, J.C. Palma, V. Ferreira, L. Culleré, Characterization of the aromatic profile of the Italia variety of Peruvian pisco by gas chromatography-olfactometry and gas chromatography coupled with flame ionization and mass spectrometry detection systems, Food Res. Int. 49 (2012) 117–125. https://doi.org/10.1016/j.foodres.2012.07.065.

[9] P. Awad, V. Athès, M.E. Decloux, G. Ferrari, G. Snakkers, P. Raguenaud, P. Giampaoli, Evolution of Volatile Compounds during the Distillation of Cognac Spirit, J. Agric. Food Chem. 65 (2017) 7736–7748. https://doi.org/10.1021/acs.jafc.7b02406.

[10] J. Ledauphin, C.L.E. Milbeau, D. Barillier, D. Hennequin, Differences in the volatile compositions of French labeled brandies (Armagnac, Calvados, Cognac, and Mirabelle) using GC-MS and PLS-DA, J. Agric. Food Chem. 58 (2010) 7782–7793. https://doi.org/10.1021/jf9045667.

[11] S. Vichi, M. Riu-Aumatell, M. Mora-Pons, S. Buxaderas, E. López-Tamames, Characterization of volatiles in different dry gins, J. Agric. Food Chem. 53 (2005) 10154–10160. https://doi.org/10.1021/jf058121b.

[12] I.W. González-Robles, D.J. Cook, The impact of maturation on concentrations of key odour active compounds which determine the aroma of tequila, J. Inst. Brew. 122 (2016) 369–380. https://doi.org/10.1002/jib.333.

[13] V. Giannetti, M.B. Mariani, F. Marini, P. Torrelli, A. Biancolillo, Flavour fingerprint for the differentiation of Grappa from other Italian distillates by GC-MS and chemometrics, Food Control. 105 (2019) 123–130. https://doi.org/10.1016/j.foodcont.2019.05.028.

[14] C.A. Faúndez, V.H. Alvarez, J.O. Valderrama, Predictive models to describe VLE in ternary mixtures water + ethanol + congener for wine distillation, Thermochim. Acta. 450 (2006) 110–117. https://doi.org/10.1016/j.tca.2006.09.005.

[15] J.D. Raal, D. Ramjugernath, Rigorous characterization of static and dynamic apparatus for measuring limiting activity coefficients, Fluid Phase Equilib. 187–188 (2001) 473–487. https://doi.org/10.1016/S0378-3812(01)00567-2.

[16] M.M. Abbott, Low-pressure phase equilibria: Measurement of VLE, Fluid Phase Equilib. 29 (1986) 193–207. https://doi.org/10.1016/0378-3812(86)85021-X.

[17] J.-N. Jaubert, R. Privat, Thermodynamic Models for Chemical Engineering: Design, Develop, Analyse and Optimize, 1st ed., ISTE Press - Elsevier, 2021.

[18] S.I. Sandler, Infinite dilution activity coefficients in chemical, environmental and biochemical engineering, Fluid Phase Equilib. 116 (1996) 343–353. https://doi.org/10.1016/0378-3812(95)02905-2.

[19] C.A. Eckert, B.A. Newman, G.L. Nicolaides, T.C. Long, Measurement and application of limiting activity coefficients, AIChE J. 27 (1981) 33–40. https://doi.org/10.1002/aic.690270107.

[20] A. Fredenslund, R.L. Jones, J.M. Prausnitz, Group- contribution estimation of activity coefficients in nonideal liquid mixtures, AIChE J. 21 (1975) 1086–1099. https://doi.org/10.1002/aic.690210607.

[21] T. Holderbaum, J. Gmehling, PSRK: A Group Contribution Equation of State Based on UNIFAC, Fluid Phase Equilib. 70 (1991) 251–265. https://doi.org/10.1016/0378-3812(91)85038-V.

[22] G.M. Wilson, Vapor-Liquid Equilibrium. XI. A New Expression for the Excess Free Energy of Mixing, J. Am. Chem. Soc. 86 (1964) 127–130.

https://doi.org/10.1021/ja01056a002.

[23] H. Renon, J.M. Prausnitz, Local compositions in thermodynamic excess functions for liquid mixtures, AIChE J. 14 (1968) 135–144. https://doi.org/10.1002/aic.690140124.

[24] H. Renon, N R T L: An empirical equation or an inspiring model for fluids mixtures properties?, Fluid Phase Equilib. 24 (1985) 87–114. https://doi.org/10.1016/0378-3812(85)87039-4.

[25] D.S. Abrams, J.M. Prausnitz, Statistical thermodynamics of liquid mixtures: A new expression for the excess Gibbs energy of partly or completely miscible systems, AIChE J. 21 (1975) 116–128. https://doi.org/10.1002/aic.690210115.

[26] J.D. Raal, D. Ramjugernath, Vapour-Liquid Equilibrium at Low Pressure, in: R.D. Weir, T.W. de Loos (Eds.), Meas. Thermodyn. Prop. Mult. Phases, International Union of Pure and Applied Chemistry, 2005: pp. 72–87.

[27] V. Athès, P. Paricaud, M. Ellaite, I. Souchon, W. Fürst, Vapour-liquid equilibria of aroma compounds in hydroalcoholic solutions: Measurements with a recirculation method and modelling with the NRTL and COSMO-SAC approaches, Fluid Phase Equilib. 265 (2008) 139–154. https://doi.org/10.1016/j.fluid.2008.01.012.

[28] S. Deterre, J. Albet, X. Joulia, O. Baudouin, P. Giampaoli, M. Decloux, V. Athès, Vapor-liquid equilibria measurements of bitter orange aroma compounds highly diluted in boiling hydro-alcoholic solutions at 101.3 kPa, J. Chem. Eng. Data. 57 (2012) 3344–3356. https://doi.org/10.1021/je3004854.

[29] I. Fichan, C. Larroche, J.B. Gros, Water solubility, vapor pressure, and activity coefficients of terpenes and terpenoids, J. Chem. Eng. Data. 44 (1999) 56–62. https://doi.org/10.1021/je980070+.

[30] D.T.C. Gillespie, Vapor-Liquid Equilibrium Still for Miscible Liquids, Ind. Eng. Chem. - Anal. Ed. 18 (1946) 575–577. https://doi.org/10.1021/i560157a018.

[31] ProSim S.A., Simulis Thermodynamics, (2021). www.prosim.net.

[32] A. Arce, A. Arce, J.M. Martínez-Ageitos, A. Soto, Isobaric vapor–liquid equilibria of 1,1-dimethylethoxy-butane+methanol or ethanol+water at 101.32kPa, Fluid Phase Equilib. 259 (2007) 57–65. https://doi.org/10.1016/j.fluid.2007.01.038.

[33] N. Kamihama, H. Matsuda, K. Kurihara, K. Tochigi, S. Oba, Isobaric Vapor–Liquid Equilibria for Ethanol + Water + Ethylene Glycol and Its Constituent Three Binary Systems, J. Chem. Eng. Data. 57 (2012) 339–344. https://doi.org/10.1021/je2008704.

[34] J.A. Riddick, W.B. Bunger, T.K. Sakano, Organic Solvents: Physical Properties and Methods of Purification, 4th editio, Wiley, New York, 1986.

[35] K. Kojima, K. Tochigi, H. Seki, K. Watase, Determination of vapor-liquid equilibriums from boiling point curves, Kagaku Kogaku. 32 (1968) 149–153.

[36] H.S. Lai, Y.F. Lin, C.H. Tu, Isobaric (vapor + liquid) equilibria for the ternary system of (ethanol + water + 1,3-propanediol) and three constituent binary systems at P = 101.3 kPa, J. Chem. Thermodyn. 68 (2014) 13–19. https://doi.org/10.1016/j.jct.2013.08.020.

[37] J. Li, E.M. Perdue, S.G. Pavlostathis, R. Araujo, Physicochemical properties of selected monoterpenes, Environ. Int. 24 (1998) 353–358. https://doi.org/10.1016/S0160-4120(98)00013-0.

[38] C. Hansch, A. Leo, D.H. Hoekman, Exploring QSAR. Hydrophobic, Electronic, and Steric Constants, American Chemical Society, Washington, DC, 1995.

[39] C. Puentes, X. Joulia, P. Paricaud, P. Giampaoli, V. Athès, M. Esteban-Decloux, Vapor-Liquid Equilibrium of Ethyl Lactate Highly Diluted in Ethanol-Water Mixtures at 101.3 kPa. Experimental Measurements and Thermodynamic Modeling Using Semiempirical Models, J. Chem. Eng. Data. 63 (2018) 365–379. https://doi.org/10.1021/acs.jced.7b00770.

[40] T.P.V.B. Dias, L.A.A.P. Fonseca, M.C. Ruiz, F.R.M. Batista, E.A.C. Batista, A.J.A. Meirelles, Vapor–Liquid Equilibrium of Mixtures Containing the Following Higher Alcohols: 2-Propanol, 2-Methyl-1-propanol, and 3-Methyl-1-butanol, J. Chem. Eng. Data. 59 (2014) 659–665. https://doi.org/10.1021/je400581e.

[41] E.C. Voutsas, C. Pamouktsis, D. Argyris, G.D. Pappa, Measurements and thermodynamic modeling of the ethanol-water system with emphasis to the azeotropic region, Fluid Phase Equilib. 308 (2011) 135–141. https://doi.org/10.1016/j.fluid.2011.06.009.

[42] S. Malanowski, Experimental methods for vapour-liquid equilibria. Part I. Circulation methods, Fluid Phase Equilib. 8 (1982) 197–219. https://doi.org/10.1016/0378-3812(82)80035-6.

[43] H. Wagenbreth, W. Blanke, Analytische Darstellung der Dichte von Äthanol-Wasser-Mischungen zur Berechnung der Interlationalen Alkoholtafeln der OIML, PTB Mitteilungen. 2/73 (1973) 90–96.

[44] International alcoholometric tables, OIML R22, International Organisation of Legal Metrology, 1975. https://www.oiml.org/en/files/pdf_r/r022-e75.pdf.

[45] A. Vetere, The Riedel Equation, Ind. Eng. Chem. Res. 30 (1991) 2487–2492. https://doi.org/10.1021/ie00059a020.

[46] L. Riedel, Eine neue universelle Dampfdruckformel Untersuchungen über eine Erweiterung des Theorems der übereinstimmenden Zustände. Teil I, Chemie Ing. Tech. 26 (1954) 83–89. https://doi.org/10.1002/cite.330260206.

[47] G.M. Wilson, C.H. Deal, Activity coefficients and molecular structure: Activity coefficients in changing environments'solutions of groups, Ind. Eng. Chem. Fundam. 1 (1962) 20–23. https://doi.org/10.1021/i160001a003.

[48] DDBST, Dortmund Data Bank. (2020). www.ddbst.com.

[49] J. Gmehling, J. Li, M. Schiller, A Modified UNIFAC Model. 2. Present Parameter Matrix and Results for Different Thermodynamic Properties, Ind. Eng. Chem. Res. 32 (1993) 178–193. https://doi.org/10.1021/ie00013a024.

[50] J. Gmehling, J. Lohmann, A. Jakob, J. Li, R. Joh, A modified UNIFAC (Dortmund) model. 3. Revision and extension, Ind. Eng. Chem. Res. 37 (1998) 4876–4882. https://doi.org/10.1021/ie980347z.

[51] P. Alessi, M. Fermeglia, I. Kikic, Significance of dilute regions, Fluid Phase Equilib. 70 (1991) 239–250. https://doi.org/10.1016/0378-3812(91)85037-U.

[52] H.E. Hughes, J.O. Maloney, The application of radioactive tracers to diffusional operations. Binary and ternary equilibrium data, Chem. Eng. Prog. 48 (1952) 192–200.

[53] J.N. Jaubert, Y. Le Guennec, A. Piña-Martinez, N. Ramirez-Velez, S. Lasala, B. Schmid, I.K. Nikolaidis, I.G. Economou, R. Privat, Benchmark Database Containing Binary-System-High-Quality-Certified Data for Cross-Comparing Thermodynamic Models and Assessing Their Accuracy, Ind. Eng. Chem. Res. 59 (2020) 14981–15027. https://doi.org/10.1021/acs.iecr.0c01734.

[54] C. Puentes, X. Joulia, V. Athès, M. Esteban-Decloux, Review and Thermodynamic Modeling with NRTL Model of Vapor-Liquid Equilibria (VLE) of Aroma Compounds Highly Diluted in Ethanol-Water Mixtures at 101.3 kPa, Ind. Eng. Chem. Res. 57 (2018) 3443–3470. https://doi.org/10.1021/acs.iecr.7b03857.

[55] R.C. Pemberton, C.J. Mash, Thermodynamic properties of aqueous non-electrolyte mixtures II. Vapour pressures and excess Gibbs energies for water + ethanol at 303.15 to 363.15 K determined by an accurate static method, J. Chem. Thermodyn. 10 (1978) 867–888. https://doi.org/10.1016/0021-9614(78)90160-X.

[56] B. Kolbe, J. Gmehling, Thermodynamic properties of ethanol + water. I. Vapour-

liquid equilibria measurements from 90 to 150°C by the static method, Fluid Phase Equilib. 23 (1985) 213–226. https://doi.org/10.1016/0378-3812(85)90007-X.

[57] A. Arce, J. Martínez-Ageitos, A. Soto, VLE for water + ethanol + 1-octanol mixtures. Experimental measurements and correlations, Fluid Phase Equilib. 122 (1996) 117–129. https://doi.org/10.1016/0378-3812(96)03041-5.

[58] V. Athès, M. Peña Y Lillo, C. Bernard, R. Pérez-Correa, I. Souchon, Comparison of Experimental Methods for Measuring Infinite Dilution Volatilities of Aroma Compounds in Water/Ethanol Mixtures, J. Agric. Food Chem. 52 (2004) 2021–2027. https://doi.org/10.1021/jf0350257.

[59] M. Tsachaki, M. Aznar, R.S.T. Linforth, A.J. Taylor, Dynamics of flavour release from ethanolic solutions, Dev. Food Sci. 43 (2006) 441–444. https://doi.org/10.1016/S0167-4501(06)80104-4.

[60] C.M. Ickes, K.R. Cadwallader, Effect of ethanol on flavor perception of Rum, Food Sci. Nutr. 6 (2018) 912–924. https://doi.org/10.1002/fsn3.629.

[61] J.M. Conner, A. Paterson, J.R. Piggott, Release of distillate flavour compounds in Scotch malt whisky, J. Sci. Food Agric. 79 (1999) 1015–1020. https://doi.org/10.1002/(SICI)1097-0010(19990515)79:7<1015::AID-JSFA321>3.0.CO;2-R.

[62] J.M. Conner, L. Birkmyre, A. Paterson, J.R. Piggott, Headspace concentrations of ethyl esters at different alcoholic strengths, J. Sci. Food Agric. 77 (1998) 121–126. https://doi.org/10.1002/(SICI)1097-0010(199805)77:1<121::AID-JSFA14>3.0.CO;2-V.

[63] M. D'Angelo, G. Onori, A. Santucci, Self-Association Behaviour of Alcohols in Diluted Aqueous Solutions (*)., Nuovo Cim. D. 16 (1994) 1499–1514. https://doi.org/10.1007%2FBF02462035.

[64] C.M. Ickes, K.R. Cadwallader, Effects of Ethanol on Flavor Perception in Alcoholic Beverages, Chemosens. Percept. 10 (2017) 119–134. https://doi.org/10.1007/s12078-017-9238-2.

[65] A. Nose, M. Hojo, Hydrogen bonding of water-ethanol in alcoholic beverages, J. Biosci. Bioeng. 102 (2006) 269–280. https://doi.org/10.1263/jbb.102.269.

[66] J.D. Raal, D. Ramjugernath, Measurement of limiting activity coefficients: Non-analytical tools, in: R.D. Weir, T.W. de Loos (Eds.), Meas. Thermodyn. Prop. Mult. Phases, International Union of Pure and Applied Chemistry, 2005: pp. 339–357. https://doi.org/10.1016/S1874-5644(05)80015-3.

[67] P. Delgado, M.T. Sanz, S. Beltrán, Isobaric vapor-liquid equilibria for the quaternary reactive system: Ethanol + water + ethyl lactate + lactic acid at 101.33 kPa, Fluid Phase Equilib. 255 (2007) 17–23. https://doi.org/10.1016/j.fluid.2007.03.022.

[68] C.A. Faúndez, F.A. Quiero, J.O. Valderrama, Thermodynamic consistency test for binary gas + water equilibrium data at low and high pressures, Chinese J. Chem. Eng. 21 (2013) 1172–1181. https://doi.org/10.1016/S1004-9541(13)60575-3.

[69] C.A. Faúndez, J.O. Valderrama, Phase equilibrium modeling in binary mixtures found in wine and must distillation, J. Food Eng. 65 (2004) 577–583. https://doi.org/10.1016/j.jfoodeng.2004.02.023.

[70] A. Arce, A. Blanco, A. Soto, I. Vidal, Densities, Refractive Indices, and Excess Molar Volumes of the Ternary Systems Water + Methanol + 1-Octanol and Water + Ethanol + 1-Octanol and Their Binary Mixtures at 298.15 K, J. Chem. Eng. Data. 38 (1993) 336–340. https://doi.org/10.1021/je00010a039.

[71] H.E. Hoga, R.B. Torres, P.L.O. Volpe, Thermodynamics properties of binary mixtures of aqueous solutions of glycols at several temperatures and atmospheric pressure, J. Chem. Thermodyn. 122 (2018) 38–64. https://doi.org/10.1016/j.jct.2018.02.022.

[72] H.A. Zarei, F. Jalili, S. Assadi, Temperature dependence of the volumetric properties of binary and ternary mixtures of water (1) + methanol (2) + ethanol (3) at ambient pressure (81.5 kPa), J. Chem. Eng. Data. 52 (2007) 2517–2526. https://doi.org/10.1021/je700300y.

[73] B. González, N. Calvar, E. Gómez, Á. Domínguez, Density, dynamic viscosity, and derived properties of binary mixtures of methanol or ethanol with water, ethyl acetate, and methyl acetate at T = (293.15, 298.15, and 303.15) K, J. Chem. Thermodyn. 39 (2007) 1578–1588. https://doi.org/10.1016/j.jct.2007.05.004.

[74] O. Redlich, A.T. Kister, Algebraic Representation of Thermodynamic Properties and the Classification of Solutions, Ind. Eng. Chem. 40 (1948) 345–348. https://doi.org/10.1021/ie50458a036.

[75] J. Wisniak, J. Ortega, L. Fernández, A fresh look at the thermodynamic consistency of vapour-liquid equilibria data, J. Chem. Thermodyn. 105 (2017) 385–395. https://doi.org/10.1016/j.jct.2016.10.038.

[76] H.C. Van Ness, S.M. Byer, R.E. Glbbs, Vapor-Liquid Equilibrium: Part I. An Appraisal of Data Reduction Methods, AIChE J. 19 (1973) 238–244.

[77] A. Fredenslund, J. Gmehling, Vapor-liquid Equilibria Using Unifac, Elsevier, Amsterdam, 1977. https://doi.org/10.1016/B978-0-444-41621-6.X5001-7.

[78] J. Wisniak, A New Test for the Thermodynamic Consistency of Vapor-Liquid Equilibrium, Ind. Eng. Chem. Res. 32 (1993) 1531–1533. https://doi.org/10.1021/ie00019a030.

[79] J.A. Larkin, Thermodynamic properties of aqueous non-electrolyte mixtures I. Excess enthalpy for water + ethanol at 298.15 to 383.15 K, J. Chem. Thermodyn. 7 (1975) 137–148. https://doi.org/10.1016/0021-9614(75)90261-X.

[80] J. Gmehling, B. Kolbe, M. Kleiber, J. Rarey, Chemical Thermodynamics for Process Simulation, Wiley-VCH, Weinheim, Germany, 2012.

[81] B. Kolbe, J. Gmehling, Thermodynamic properties of ethanol + water II. Potentials and limits of GE models, Fluid Phase Equilib. 23 (1985) 227–242. https://doi.org/10.1016/0378-3812(85)90008-1.

[82] X. Zhang, X. Hao, C. Jian, H. Wang, W. Kong, G. Shangguan, M. Xia, Experimental isobaric vapour-liquid equilibrium data for binary systems of {sec-butyl acetate (SBAC) + acetamide} and {sec-butyl alcohol (SBA) + acetamide} and the ternary system of (SBAC + SBA + acetamide) at 101.3 kPa, J. Chem. Thermodyn. 144 (2020) 106087. https://doi.org/10.1016/j.jct.2020.106087.

[83] V. Gomis, M.D. Saquete, A. Font, J. García-Cano, I. Martínez-Castellanos, Phase equilibria of the water + 1-butanol + 2-pentanol ternary system at 101.3 kPa, J. Chem. Thermodyn. 123 (2018) 38–45. https://doi.org/10.1016/j.jct.2018.03.024.

[84] G. Rubio-Pérez, N. Muñoz-Rujas, A. Srhiyer, E.A. Montero, F. Aguilar, Isobaric vapor-liquid equilibrium, density and speed of sound of binary mixtures 2,2,4-trimethylpentane + 1-butanol or dibutyl ether (DBE) at 101.3 kPa, Fluid Phase Equilib. 475 (2018) 10–17. https://doi.org/10.1016/j.fluid.2018.07.027.

[85] B.E. Poling, J.M. Prausnitz, J.P. O'Connell, The Properties of Gases and Liquids, 5th ed., McGraw–Hill, New York, 2001.